The baryon fraction of ΛCDM haloes

Robert A. Crain[1]⋆, Vincent R. Eke[1], Carlos S. Frenk[1], Adrian Jenkins[1],
Ian G. McCarthy[1], Julio F. Navarro[2] & Frazer R. Pearce[3]

[1] *Institute for Computational Cosmology, Department of Physics, University of Durham, South Road, Durham, DH1 3LE, UK*
[2] *Department of Physics & Astronomy, University of Victoria, Victoria, British Columbia, V8P 1A1, Canada*
[3] *School of Physics & Astronomy, University of Nottingham, University Park, Nottingham, NG7 2RD, UK*

6 January 2014

arXiv:astro-ph/0610602v1 19 Oct 2006

ABSTRACT

We investigate the baryon fraction in dark matter haloes formed in non-radiative gas-dynamical simulations of the ΛCDM cosmogony. By combining a realisation of the *Millennium Simulation* (Springel et al.) with a simulation of a smaller volume focussing on dwarf haloes, our study spans five decades in halo mass, from $10^{10}\ h^{-1}$ M$_\odot$ to $10^{15}\ h^{-1}$ M$_\odot$. We find that the baryon fraction within the halo virial radius is typically 90% of the cosmic mean, with an rms scatter of 6%, independently of redshift and of halo mass down to the smallest resolved haloes. Our results show that, contrary to the proposal of Mo et al. (2005), pre-virialisation gravitational heating is unable to prevent the collapse of gas within galactic and proto-galactic haloes, and confirm the need for non-gravitational feedback in order to reduce the efficiency of gas cooling and star formation in dwarf galaxy haloes. Simulations including a simple photo-heating model (where a gas temperature floor of $T_{\rm floor} = 2 \times 10^4$ K is imposed from $z = 11$) confirm earlier suggestions that photoheating can only prevent the collapse of baryons in systems with virial temperatures $T_{200} \lesssim 2.2\,T_{\rm floor} \approx 4.4 \times 10^4$ K (corresponding to a virial mass of $M_{200} \sim 10^{10}\ h^{-1}$ M$_\odot$ and a circular velocity of $V_{200} \sim 35$ km s^{-1}). Photoheating may thus help regulate the formation of dwarf spheroidals and other galaxies at the extreme faint-end of the luminosity function, but it cannot, on its own, reconcile the abundance of sub-$L_\star$ galaxies with the vast number of dwarf haloes expected in the ΛCDM cosmogony. The lack of evolution or mass dependence seen in the baryon fraction augurs well for X-ray cluster studies that assume a universal and non-evolving baryon fraction to place constraints on cosmological parameters.

Key words:

1 INTRODUCTION

In the current paradigm of cosmic evolution, the ΛCDM model, structures grow from an initially smooth density field into a rich network of filaments and haloes. Initially, baryons approximately follow the collisionless dark matter, but the two components evolve differently in non-linear regions after recombination. In proto-galactic haloes, for example, the kinetic energy of the collapse is thermalised in shocks by the baryons, but rapid radiative cooling losses allow for further collapse, leading to the formation of dense gaseous discs susceptible to swift transformation into stars (White & Rees 1978).

The efficient gas cooling that accompanies the collapse of protogalactic haloes at high redshift underlies one of the central apparent conflicts between hierarchical models of structure formation and observation. Indeed, Cole (1991) and White & Frenk (1991) highlighted that, in the absence of additional physics, hierarchi-

cal models predict that essentially the entire baryonic content of the Universe should have cooled at high redshift and, presumably, turned into stars by the present epoch. This is in strong contradiction with observations, which suggest that stars make up less than 5% of the baryons in the Universe (for a review, see Balogh et al. 2001). To avoid this 'cooling catastrophe', models of galaxy formation frequently invoke various astrophysical mechanisms that counteract cooling and, in some cases, reheat cold gas.

One consequence of the cooling catastrophe is the difficulty in reconciling the galaxy luminosity function with the ΛCDM halo mass function. This was recognised in the pioneering work of White & Rees (1978), and it is now widely accepted that a heating mechanism (usually referred to as 'feedback') is required to explain the reduced star formation efficiency required to match the shallow faint end, as well as the sharp cut-off at the bright end, of the galaxy luminosity function (e.g. Kauffmann et al. 1999; Somerville & Primack 1999; Cole et al. 2000; Benson et al. 2003; Bower et al. 2006; Croton et al. 2006)

The main heating mechanisms are commonly believed to be:

⋆ E-mail: r.a.crain@durham.ac.uk

(i) photo-heating by the energetic photons that reionised the Universe at high redshift, (ii) the thermal and kinetic output of evolving stars and supernovae (SNe), and (iii) the energy released by accretion of matter into the supermassive black holes responsible for active galactic nuclei (AGN). The importance of each of these processes varies as a function of halo mass. Whereas (i) is thought to curtail star formation in extremely low-mass haloes and substructures, (ii) is assumed to regulate the star formation history of dwarf and normal galaxies. The role of (iii) is expected to be most relevant for the formation of giant galaxies, typically ellipticals found predominantly in the dense cores of galaxy clusters (e.g Richstone et al. 1998).

Of all these, mechanism (ii) is the best studied, but there is still no consensus concerning its role in regulating star formation. Although it is energetically possible for SNe to suppress star formation in galactic haloes (Dekel and Silk 1986, White and Frenk 1991), it has long been recognised that the efficiency required for this process to be viable is uncomfortably high (Benson et al. 2003; Kang et al. 2005). Hydrodynamical simulations, for example, show that under normal circumstances SNe are far less efficient at expelling mass and reheating the IGM than required by galaxy formation models in order to match the faint-end of the luminosity function (Mac Low & Ferrara 1999; Strickland & Stevens 2000). Identifying an additional or alternative source of feedback is therefore highly desirable.

In a recent paper, Mo et al. (2005, hereafter M05) proposed an elegant alternative, namely, that the collapse of large-scale pancakes and filaments might heat the gas prior to the assembly of low-mass haloes. M05 sketch analytic arguments in support of the idea that this 'pre-virialisation' gravitational heating might generate enough entropy, at low redshift ($z \lesssim 2$), to inhibit substantially the accretion of gas into low-mass haloes. If efficient enough, this mechanism may offer a simple and attractive resolution to the cooling crisis, and a possible explanation of the form of the faint end of the galaxy luminosity function without the need to invoke feedback from non-gravitational sources, such as photoionisation or SNe.

This is clearly an intriguing proposition, and we present here a suite of cosmological gas-dynamical simulations aimed at assessing the viability of the pre-virialisation heating hypothesis in the ΛCDM cosmogony. Our simulations allow us to probe a vast range of halo masses, from $10^{10} \ h^{-1} \ \mathrm{M}_\odot$ to roughly $10^{15} \ h^{-1} \ \mathrm{M}_\odot$. The simulations assume that baryons evolve as a non-radiative fluid; this is a conservative assumption when testing the pre-virialisation hypothesis, as radiative losses would only serve to facilitate the collapse of baryons into protogalactic haloes.

We also use the same suite of simulations to explore the baryon fraction at the opposite end of the halo mass function, i.e., in galaxy cluster haloes. Adopting a non-radiative gas approach is a reasonable simplification here, since the majority of the intracluster medium (ICM) has a cooling time that exceeds the age of the Universe. The most massive galaxy clusters are of particular cosmological interest since their baryon fractions are expected to trace accurately the cosmic mean. Indeed, the comparison of cluster baryon fractions (f_b) with the baryon density parameter (Ω_b) implied by Big-Bang nucleosynthesis calculations provides decisive evidence for a Universe with (dark) matter density well below the critical density for closure (White et al. 1993).

In addition, the apparent redshift dependence of cluster baryon fractions can be used to constrain the geometry of the Universe (Sasaki 1996), its deceleration (Pen 1997), and by extension, the dark energy equation of state (Allen et al. 2004). These tests exploit the redshift dependence of angular diameter distances and rely on

cluster baryon fractions being roughly universal and non-evolving over the redshift range where they can be observed (typically $z < 1$).

Our simulation suite provides the largest sample of haloes with non-radiative gas dynamics reported to date. This allows us to investigate the mass dependence, evolution and dispersion of halo baryon fractions with unprecedented statistical reliability. These results can be used to test critically the viability of the pre-virialisation heating hypothesis and to examine the stability and evolution of cluster baryon fractions.

In the following section we describe our simulation suite, and in Section 3 we outline our analysis methods and main results. We discuss them in Section 4 and conclude with a brief summary in Section 5.

2   SIMULATION DETAILS

To maximise the dynamic range of our halo sample we analyse two simulations of different volumes. One (labelled LOW-MASS) is a high-resolution 'zoomed-in' simulation of a relatively small volume designed to study low-mass haloes. The other (HIGH-MASS) is a gas-dynamical realisation of the *Millennium Simulation* (Springel et al. 2005), a large volume containing many well resolved galaxy clusters. We address numerical convergence issues by simulating the collapse of a 'pancake' at varying numerical resolution. And, finally, we test explicitly the robustness of our results in the LOW-MASS simulation by re-simulating at much higher resolution a single (DWARF) halo with virial mass $10^{10} \ h^{-1} \ \mathrm{M}_\odot$. The numerical parameters and other details of the simulations are listed in Table 1.

We evolve our initial conditions in all cases using the publicly available parallel code GADGET-2 (Springel 2005), with non-radiative[1] baryon physics implemented by smoothed particle hydrodynamics (SPH).

2.1   HIGH-MASS simulation

Our sample of high-mass haloes is drawn from a non-radiative gas-dynamical realisation of the *Millennium Simulation*. It adopts the same displacement field and cosmology as the original simulation, but has lower mass resolution: 5×10^8 gas and dark matter particles within a periodic simulation box of side $500 \ h^{-1}$ Mpc. The baryon density parameter $\Omega_\mathrm{b} = 0.045$ results in particle masses of $m_\mathrm{gas} = 3.12 \times 10^9 \ h^{-1} \ \mathrm{M}_\odot$; for the dark matter we adopt $\Omega_\mathrm{dm} = 0.25$, implying a particle mass of $m_\mathrm{dm} = 1.42 \times 10^{10} \ h^{-1} \ \mathrm{M}_\odot$. We choose a comoving gravitational softening of $100 \ h^{-1}$ kpc until $z = 3$, at which point it is fixed in physical units to $25 \ h^{-1}$ kpc. Further details and analysis of this simulation shall be presented in a forthcoming paper (Pearce et al., *in prep*).

2.2   LOW-MASS simulation

In order to analyse a representative region of the Universe whilst still resolving low mass haloes, we simulate the evolution of a spherical region of radius $7 \ h^{-1}$ Mpc, identified at $z = 0$ in a simulation of a box $100 \ h^{-1}$ Mpc on a side with the same cosmological parameters as the *Millennium Simulation*. The sphere was

---

[1] We avoid the common practice of terming non-radiative simulations 'adiabatic', since they include non-adiabatic shocks.

	m_{gas} $[h^{-1}\,\mathrm{M_\odot}]$	m_{dm} $[h^{-1}M_\odot]$	N_{p}	ϵ_{com} $[h^{-1}\,\mathrm{kpc}]$	Ω_{b}	Ω_0	L $[h^{-1}\,\mathrm{Mpc}]$	z_{init}
HIGH-MASS	3.12×10^9	1.42×10^{10}	5.0×10^8	100.0^*	0.045	0.25	500	49
LOW-MASS	1.65×10^6	8.70×10^6	2.6×10^6	5.0	0.040	0.25	100	127
DWARF	1.20×10^4	7.80×10^4	3.4×10^5	0.4	0.040	0.30	35.325	74
PANCAKE	1.20×10^6	7.83×10^6	3.5×10^5	10.0	0.040	0.30	N/A	145

Table 1. Parameters for the various simulations. Note that each simulation contained an equal number, N_{p}, of both gas and high-resolution dark matter particles. Softening lengths, ϵ, are quoted in comoving coordinates hence we mark the HIGH-MASS simulation with an asterisk to denote that its softening was switched to physical units at $z = 3$. The PANCAKE simulation has no boxsize, L, since it was run with vacuum boundary conditions.

chosen at random from a sample of spherical regions with mean density within 10% of the cosmic mean, and devoid of haloes with mass $M_{200} > 10^{13}\,h^{-1}\,\mathrm{M_\odot}$, in order to prevent the region from being dominated by a single halo. Randomly placed spheres satisfy the density selection criterion slightly less than 10% of the time, since the volume is dominated by underdense regions. Approximately one-third of spheres satisfying the density criterion lack haloes more massive than $10^{13}\,h^{-1}\,\mathrm{M_\odot}$.

Our initial conditions are generated by resampling the region with a greater number of particles and adding additional short wavelength perturbations, whilst coarse sampling the external mass distribution with multi-mass collisionless particles to reproduce the large-scale gravitational field. Our resampling algorithm is based upon the procedure outlined by Frenk et al. (1996), and is described in detail by Power et al. (2003). Gas is added to the high-resolution region by splitting each particle into a dark matter particle and a gas particle, with mass ratio given by the adopted baryon and dark matter density parameters. This implies that each gas particle has a corresponding dark matter 'partner' associated with a unique volume element at high redshift, a useful feature when tracing the differences in the evolution of the two components in the non-linear regime.

The LOW-MASS simulation features 2.5×10^6 gas particles of masses $m_{\mathrm{gas}} = 1.65 \times 10^6\,h^{-1}\,\mathrm{M_\odot}$ and an equal number of high resolution dark matter particles, of mass $m_{\mathrm{dm}} = 8.70 \times 10^6\,h^{-1}\,\mathrm{M_\odot}$. At this resolution, the simulated volume yields a sample of ~ 1300 well resolved (i.e., $N_{\mathrm{dm}} > 150$) low mass haloes at $z = 0$ whilst remaining relatively computationally inexpensive.

2.3 DWARF simulation

In order to assess the robustness of our results for low-mass haloes we re-simulate a single dwarf halo ($10^{10}\,h^{-1}M_\odot$) at much higher resolution than its counterparts in LOW-MASS. Because pre-virialisation heating is expected to be most effective in haloes assembling late, we select for resimulation a dwarf halo with relatively late formation time for its mass. The most massive progenitor first exceeds half the final mass of the halo at $z = 0.6$, whilst the extensions to the Press-Schechter theory (Press & Schechter 1974) described by Lacey & Cole (1993) suggest that the most probable formation time for a halo of this mass is $z \sim 2$.

We selected the halo from a parent simulation of box length $35.325\,h^{-1}$ Mpc and density parameters $(\Omega_{\mathrm{m}}, \Omega_\Lambda = 0.3, 0.7)$. We apply the same resimulation technique as for LOW-MASS, using 3.4×10^5 gas and high-resolution dark matter particles. We adopt a baryon density parameter of $\Omega_{\mathrm{b}} = 0.04$, which implies particle masses of $m_{\mathrm{gas}} = 1.20 \times 10^4\,h^{-1}\,\mathrm{M_\odot}$ and $m_{\mathrm{dm}} = 7.8 \times 10^4\,h^{-1}\,\mathrm{M_\odot}$. At $z = 0$, the halo has mass $M_{200} = $

$9.5 \times 10^9\,h^{-1}\,\mathrm{M_\odot}$, virial radius $r_{200} = 34.5\,h^{-1}$ kpc, and circular velocity $V_{200} = 35$ km s^{-1}.

2.4 PANCAKE simulation

The pre-virialisation mechanism outlined by M05 assumes that gas is heated during the pancake-like collapse of the large-scale structure within which dwarf haloes are embedded. It is therefore important to explore whether our numerical techniques are suitable to describe this process accurately, as well as whether the results are not artificially marred by limited numerical resolution.

We investigate this by simulating the collapse of an idealised pancake with similar numerical resolution as that of the LOW-MASS simulation, and then vary the resolution in order to assess convergence. The simulation involves the collapse of a uniform spherical region of mass $3 \times 10^{12}\,h^{-1}\,\mathrm{M_\odot}$, initially perturbed so that it collapses along one axis to form a flattened pancake at $z = 2$. We use a 'glass' rather than a grid in order to minimise the artifacts introduced by anisotropies in the grid. The desired dynamics are achieved by compressing the sphere along one axis and expanding it by half of the compression factor along the other two axes, with initial velocities computed using linear theory.

The choice of parameters for this simulation is motivated by the discussion of M05, who argue that such 'pancakes' might represent the typical environment where dwarf galaxy halos are formed, and that pre-virialisation heating might have been missed in early simulations because of inadequate resolution. As noted by M05, a collapsing pancake forms shocks on both sides, so a faithful treatment of its thermodynamic evolution requires $\gtrsim 8$ smoothing lengths across its collapsing axis. Following M05, and assuming that shocks operate as the collapsed structure approaches an overdensity of ~ 10, this implies a pancake thickness of $200\,h^{-1}$ kpc (comoving) and a minimum resolution of $25\,h^{-1}$ kpc, again comoving. We fulfil this criterion using a particle mass similar to that of the LOW-MASS simulation. At an overdensity of $10\,\Omega_{\mathrm{b}}\rho_{\mathrm{c}}(z)$ a mass of $40\,m_{\mathrm{p}}$ particles (comparable to what is used to define the SPH smoothing length scale) is contained within a sphere of comoving smoothing length $h_{\mathrm{sml}} \sim 25\,h^{-1}$ kpc.

3 ANALYSIS & RESULTS

Figure 1 shows various snapshots of the LOW-MASS simulation. Each box is $10\,h^{-1}$ Mpc on a side and shows the positions of gas particles, colour-coded according to density. This figure shows clearly the highly anisotropic nature of the large-scale structure, but also highlights the points that many dwarf dark matter halos had already collapsed by $z \sim 2$. As we discuss below, this has important
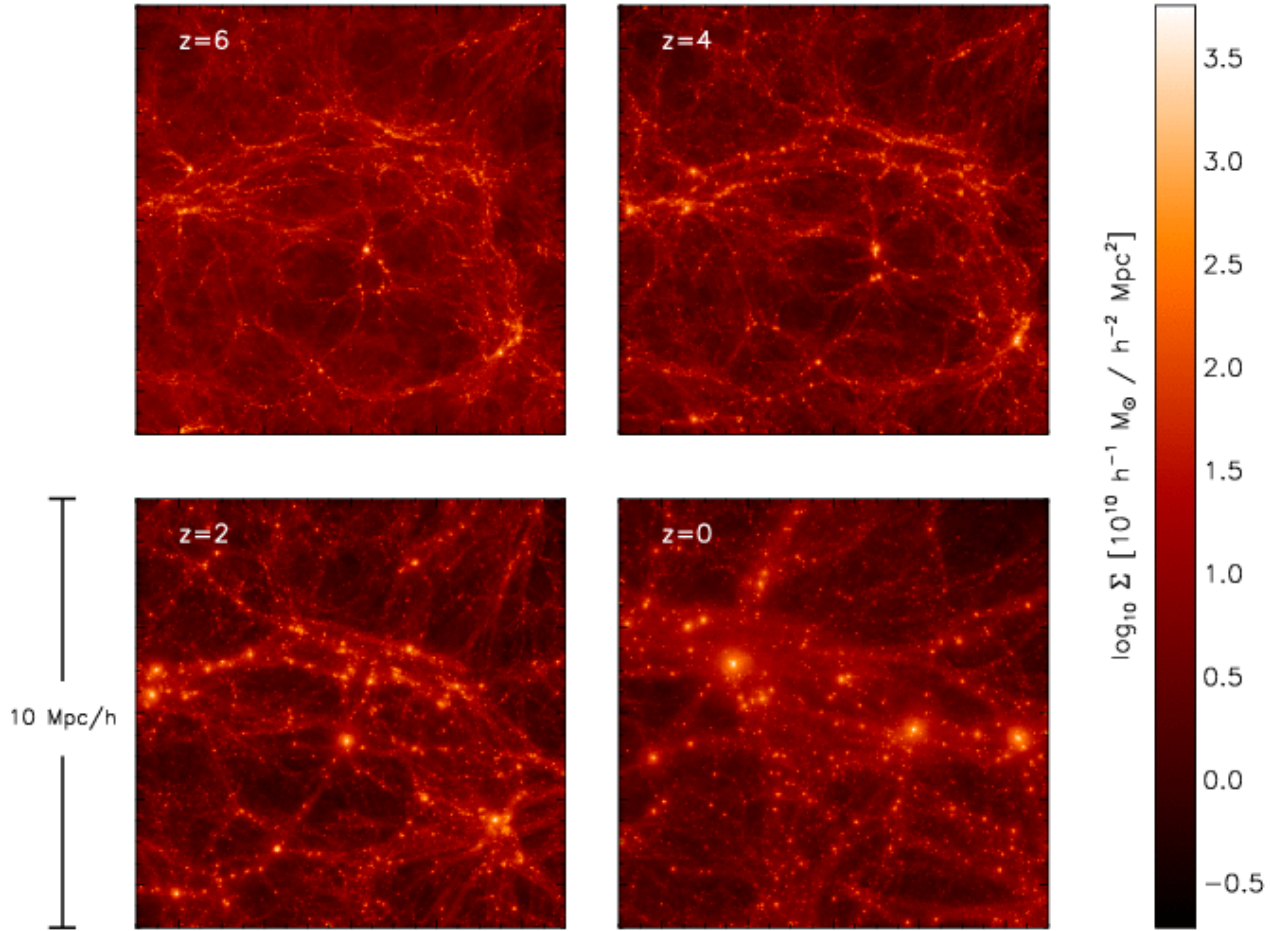
Figure 1. Redshift-progression of the projected gas density within a cube of side $10\ h^{-1}$ Mpc (comoving) in the LOW-MASS simulation. The progression clearly illustrates that by $z = 2$ many dark matter haloes have already collapsed, driving their associated gas to high overdensities. Such gas is afforded stability against the shocks that develop as the large-scale environment, within which it is embedded, collapses into pancakes and filaments

implications for the efficiency of pre-virialisation heating and its effects on the baryon fraction of collapsed systems.

3.1 Halo finding algorithm

We use a friends-of-friends group finding algorithm (Davis et al. 1985) with a short linking length ($b = 0.05$) to locate the cores of haloes in the simulation volumes. The centres of these haloes are used as starting points for an iterative algorithm that finds spherically overdense regions of mean enclosed density $200\rho_{crit}(z)$, whose centres coincide with their centres of mass. We define the virial radius, r_{200}, as the radius of this sphere. Other 'virial' quantities quoted for haloes refer to measurements within this radius, unless otherwise specified.

We consider only haloes with at least 150 dark matter particles in order to minimise the effects of poor numerical resolution, and clean the sample by removing haloes partially contained within other haloes. In the case of LOW-MASS we also disregard haloes located closer than $200\ h^{-1}$ kpc from the boundary of the resimu-

lated region at $z = 0$, since they may have been subject to boundary effects.

3.2 Baryon fractions

3.2.1 HIGH-MASS

The right-hand panels of Figure 2 show the baryon fraction in haloes identified in the HIGH-MASS simulation at $z = 1$ and at $z = 0$. These panels show the largest sample of haloes simulated with non-radiative gas physics reported to date, with approximately $49,500$ and $115,000$ haloes resolved at $z = 1$ and $z = 0$ respectively. The panels show that the baryon fraction is independent of mass, and has not evolved at least since $z = 1$, the highest redshift for which cluster baryon fractions can be estimated reliably from X-ray observations (e.g. the observations of Allen et al. (2004) span the redshift range $0.07 < z < 0.9$).

The mean cluster baryon fraction within the virial radius is approximately 90% of the cosmic mean, with relatively small scatter; the root-mean-square dispersion is less than 3% for haloes of
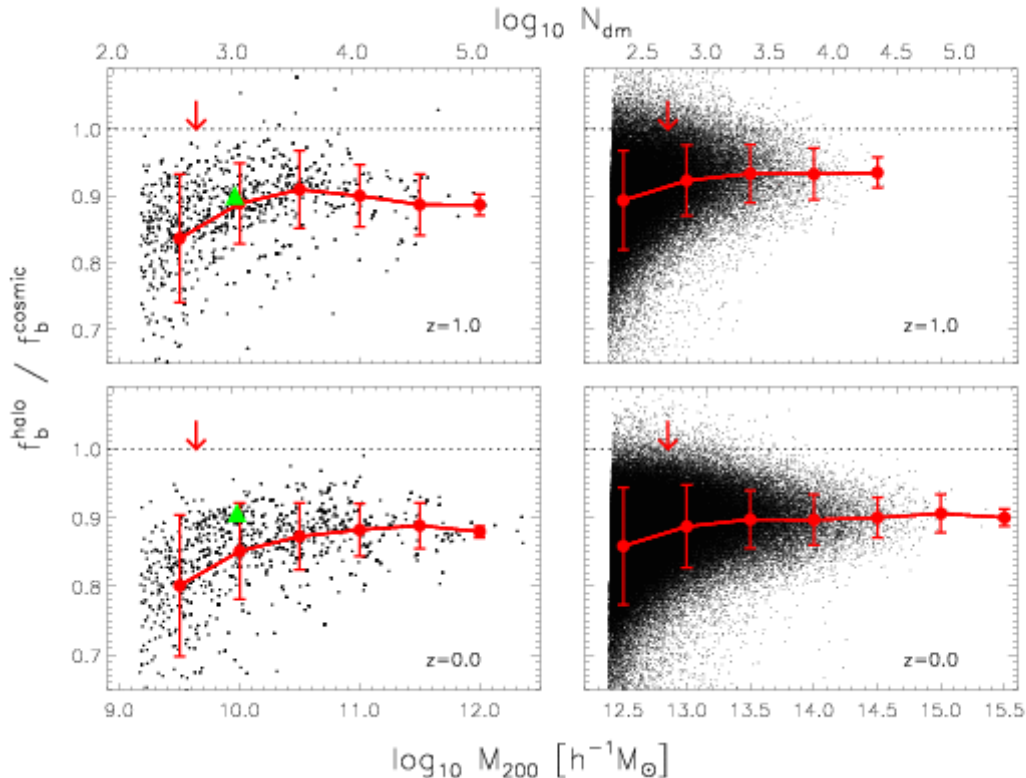
Figure 2. Baryon fractions, in units of the universal value, of well resolved haloes ($N_{\rm dm} > 150$) drawn from the LOW-MASS (*left-hand panels*) and HIGH-MASS (*right-hand panels*) simulations at $z = 1$ (*upper panels*) and $z = 0$ (*lower panels*). The large dots and error bars show the mean and rms of the distribution, respectively. The green triangle marks the baryon fraction of the halo in the DWARF simulation. The upper horizontal axis gives the equivalent number of dark matter particles at a given mass scale. The downward arrows in each plot illustrate the mass scale corresponding to 500 dark matter particles.

mass $M_{200} \gtrsim 3 \times 10^{14}\ h^{-1}\ {\rm M}_\odot$, and the difference between the $10^{\rm th}$ and $90^{\rm th}$ percentiles is always less than 7.5% over the same mass range. The scatter remains small for all well resolved haloes; the rms scatter is less than 6% for haloes resolved by at least 500 dark matter particles. This result is in broad agreement with previous simulations of cluster baryon fractions in the non-radiative regime using SPH codes (e.g. Navarro et al. 1995; Eke et al. 1998; Frenk et al. 1999; Ettori et al. 2006).

These results are only weakly dependent on radius; within a radius encompassing a mean inner density 500 times greater than critical, r_{500}, the results are very similar to those within r_{200}: for $M_{200} \gtrsim 3 \times 10^{14}\ h^{-1}\ {\rm M}_\odot$ the baryon fraction remains, on average, 90% with an rms dispersion of 3%. This radius, which is $\sim 0.7 r_{200}$ for an NFW profile (Navarro et al. 1996, 1997) with concentration $c = 5$, is roughly the maximum radius for which total cluster masses can be estimated reliably from X-ray observations (e.g. Vikhlinin et al. 2006).

3.2.2 LOW-MASS

The left-hand panels of Figure 2 show that a similar result applies to the halo sample identified in the LOW-MASS simulation. The baryon fraction of galactic and dwarf haloes is also about 90% of the cosmic mean, and shows no discernible dependence on mass or redshift.

A noticeable downturn is observed below about $10^{10}\ h^{-1} M_\odot$, but this may be ascribed to the poorer resolution affecting such haloes, since an underestimate of the gas density at accretion

shocks leads to artificially high post-shock entropies. Note that a similar downturn is also seen in the HIGH-MASS sample for haloes resolved with fewer than ~ 500 particles. Downward arrows show the mass scale corresponding to 500 dark matter particles in each simulation.

3.2.3 DWARF

Figure 2 suggests that for haloes resolved with more than $\sim 500 - 1000$ particles, numerical resolution does not affect the measured baryon fractions. Further supporting evidence comes from the results obtained for the high resolution individual DWARF halo. These are shown in Figure 2 with a filled triangle, and are consistent with LOW-MASS haloes of similar mass.

3.2.4 PANCAKE

One may still worry that, despite the apparent convergence of the results shown in Figure 2, the numerical resolution is insufficient to capture the shocks during the pancake collapse phase that accompanies the formation of haloes. We can test this by examining the PANCAKE simulation.

Figure 3 shows the evolution of the entropy (measured by $s = T/n_{\rm e}^{2/3}$), and of the temperature of the gas during the collapse of the sphere to a pancake configuration. Note that when computing the electron density, $n_{\rm e}$, we assume the gas is fully ionised and of primordial composition. At $z = 2$ the system reaches maximum asphericity, and is well described by a plane of comoving thickness
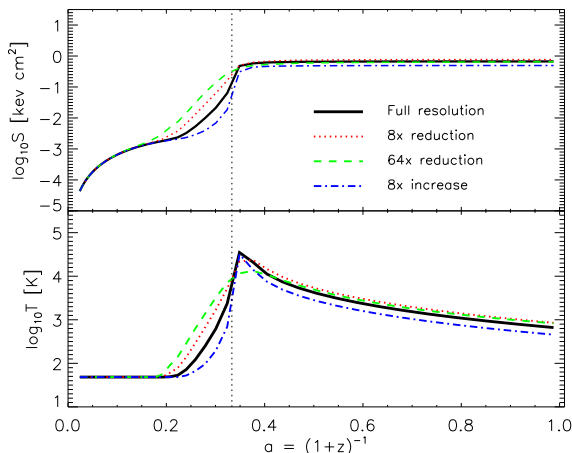
Figure 3. The evolution of the median entropy parameter (*top*) and median temperature (*bottom*) of gas particles within the PANCAKE collapse simulation. The solid line in each case represents the simulation featuring particle mass resolution identical to the LOW-MASS simulation. We supplement this run with degraded resolution runs with particle number reduced by a factor of 8 (*dotted line*) and 64 (*dashed line*). An improved resolution run is also presented, with particle number a factor of 8 greater (*dot-dashed line*). The vertical dotted line marks $z = 2$.
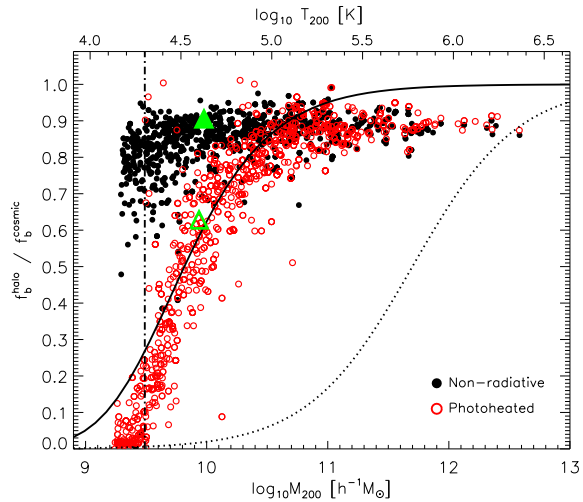

Figure 4. Baryon fractions, in units of the universal value, at $z = 0$ for the LOW-MASS simulation with and without our photoionising background model. The open and solid green triangles show the baryon fraction of the DWARF halo with and without the same model, whilst the vertical dot-dashed line marks the virial mass and virial temperature equating to the temperature floor. The solid line denotes the baryon fractions predicted by M05 for haloes in the presence of a UV background, whilst the dotted line shows the prediction of the M05 gravitational preheating model.

$25\ h^{-1}$ kpc (c.f. comoving softening of $10\ h^{-1}$ kpc) and comoving radial extension of $1.5\ h^{-1}$ Mpc.

The collapse heats gas to a median temperature of 3×10^4 K, and the median specific entropy reaches $s \simeq 1$ keV cm^2. We test explicitly the effect of resolution by re-running the PANCAKE simulation with particle numbers reduced by factors of 8 and 64 relative to the standard resolution of LOW-MASS; we complete the resolution study by running a higher-resolution case where the number of particles was increased by a factor of 8. Gravitational softenings were scaled as $\epsilon \propto N_{\rm P}^{1/3}$.

As shown in Figure 3 the post-shock median entropy and temperature jumps are quite insensitive to numerical resolution, although the transition becomes noticeably sharper as the resolution increases. This test shows that limited resolution does not lead to a substantial underestimate of the entropy jump in numerical simulations of pancake-like collapse. Actually, poor resolution leads typically to underestimation of the true densities: entropies are therefore typically *overestimated* in poor resolution simulations. This result, together with the consistency between the LOW-MASS and DWARF simulations, gives us confidence that baryon fractions in our simulations are not unduly affected by resolution effects.

3.3 Photoheating

The one feedback mechanism that is certainly present at early times is associated with the energetic photons that reionised the Universe at high redshift. This has long been recognised as having the potential to inhibit the formation of galaxies in low-mass haloes, although there is still no consensus concerning the mass scale below which photoheating becomes effective at halting galaxy formation (Blumenthal et al. 1984; Efstathiou 1992; Quinn et al. 1996; Bullock et al. 2000; Benson et al. 2002). Most semianalytic galaxy formation models have so far adopted the prescription of Gnedin (2000) to determine the gas accreted by haloes for given IGM pres-

sure, but recent results presented by Hoeft et al. (2006) suggest that Gnedin's approach may substantially overestimate the mass scale of photoheating.

This motivates us to include a simple photoionisation heating model in our simulations. The aim is twofold. On the one hand, we wish to shed light on the disagreement about the effects of photoheating on gas fractions, but, on the other hand, we would also like to explore whether photoheating may act to suppress the efficiency of gas accretion in the early phases of the hierarchy, facilitating and enhancing the thermodynamic effect of pancake-driven shocks.

We investigate the combined effect of gravitational and photoheating by re-running the DWARF and LOW-MASS simulations, again with non-radiative gas physics, but, motivated by the third-year *WMAP* data (Spergel et al. 2006), imposing a spatially uniform temperature floor for all gas particles at $z = 11$. To aid as much as possible the pre-virialisation generation of entropy, we adopt for the temperature floor a rather high value, $T_{\rm floor} = 2 \times 10^4$ K, consistent with the maximum temperature of the IGM at mean density, as probed by QSO absorption spectra (Schaye et al. 2000).

This should clearly impact gas accretion on dwarf galaxy haloes and, in particular, our DWARF halo, where the virial temperature is only $\sim 4.4 \times 10^4$ K at $z = 0$, only a factor of 2.2 above $T_{\rm floor}$. We therefore expect that a considerable fraction of the gas bound to small halo progenitors at high redshift should be photo-evaporated from this structure.

Figure 4 illustrates the effect of the additional heating on the baryon fractions of the LOW-MASS halo sample (open circles) and compares them with the results of the non-radiative run (filled circles). Photoheating introduces a well-defined mass scale below which gas accretion is strongly suppressed. Below $M_{200} \sim 10^{10}\ h^{-1}$ M$_\odot$ haloes are able to retain less than one half of their share of baryons within their virial radii; the effect is as large as 90% in haloes below $3 \times 10^9\ h^{-1}$ M$_\odot$, corresponding to an effec-
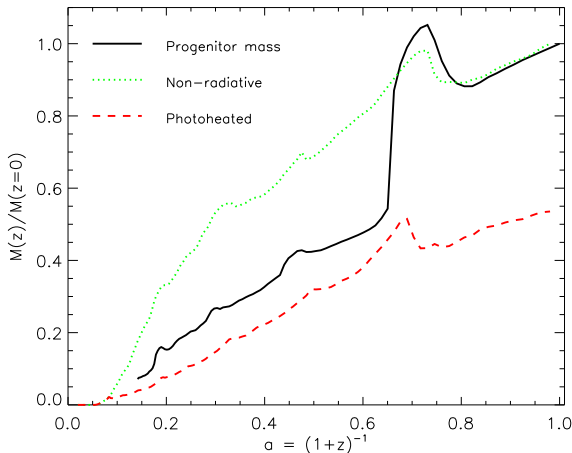
Figure 5. A comparison of the evolution of the mass of the main DWARF halo progenitor (*black solid line*), with the evolution of the final halo gas mass that is already collapsed at redshift z, as defined by the condition that its density exceeds $10\rho_c(z)$ (*green dotted line*). The data are normalised to their values at $z = 0$. The latter quantity is also shown for the case when our photoheating treatment is applied (*red dashed line*), this time normalised to the $z = 0$ value of the purely non-radiative case.

tive virial temperature very similar to the photoheating temperature floor.

4 DISCUSSION

The main result of the previous section is that, in the non-radiative approximation, the baryon fraction of ΛCDM haloes is independent of redshift as well as of mass, in the range resolved by our simulations (10^{10}-10^{15} h^{-1} M$_\odot$). Photoionisation reduces the baryon fraction only in haloes with virial temperature comparable to that imposed by the ionising photons, typically just above 10^4 K. We discuss below the implication of these results for models of galaxy formation and for the interpretation of observations of baryon fractions in clusters.

4.1 Baryon fraction bias

The lack of dependence of baryon fractions on halo mass is intriguing, as is the fact that the mean value within the virial radius is only $\sim 90\%$ of the cosmic mean. The same result has been observed in other simulations (Navarro et al. 1995; Eke et al. 1998; Frenk et al. 1999), and has been ascribed to the collisional *vs.* collisionless nature of the baryons and dark matter, coupled to the hierarchical assembly of haloes in the ΛCDM cosmogony. Indeed, during the many mergers that mark the formation of a halo, shocks act to stop the gas whilst the dark matter streams through freely. This leads to a temporary spatial offset between dark and gaseous components during which energy and angular momentum are transferred from the dark matter to the baryons, as discussed in detail by Navarro & White (1993). The energy gained during mergers results in a more extended gaseous component, and an overall (slight) reduction in the baryon fraction relative to the cosmic mean.

4.2 Pre-virialisation heating

The results of Figure 2 imply that pre-virialisation heating is ineffective at preventing the collapse of baryons into low-mass haloes, even for masses as low as 10^{10} h^{-1} M$_\odot$. Figure 4 compares the baryon fractions of LOW-MASS haloes at $z = 0$ (filled circles) with the predictions of the M05 model (dotted line). M05 argue that the IGM in low-mass haloes should have been heated by shocks to roughly ~ 10 kev cm^2 prior to halo assembly, and that this would lead to a reduction of $\gtrsim 50\%$ in the baryons filling haloes of mass $< 6 \times 10^{11}$ h^{-1} M$_\odot$. M05 propose a fitting formula to characterise this effect;

$$\frac{f_b^{halo}}{f_b^{cosmic}} = \frac{1}{(1 + M_c/M)^\alpha} \qquad (1)$$

where $\alpha = 1$ and $M_c = 5 \times 10^{11}$ h^{-1} M$_\odot$ is a characteristic mass scale. This function clearly fails to reproduce our results, and suggests that the hypotheses on which M05 base their model are not satisfied in our simulations.

The main premise of M05's model is that most low-mass haloes form in extremely aspherical regions where their assembly might be delayed, allowing for pancake-driven shocks to elevate the entropy of the IGM prior to halo assembly. Our simulations, however, indicate otherwise.

Firstly, low-mass haloes surviving to the present were, at the time of their formation, in regions where pre-virialisation shocks were weaker than envisaged by M05. For example, we find a typical post-collapse entropy of ~ 1 keV cm^2 in our pancake collapse simulations, about an order of magnitude lower than adopted by M05 to compute the model shown by the dotted curve in Figure 4. These results suggest that the halo assembly process is approximately scale-free; if pre-virialisation heating does indeed occur, it affects *all* haloes in similar measure, leaving no particular signature in low-mass haloes.

Secondly, the material destined to make a low-mass halo collects into dense, early-collapsing clumps prior to the collapse of the surrounding 'pancake'. The pancake, in other words, is not a nearly uniform aspherical structure where shocks may propagate freely, but rather a large-scale feature where a substantial fraction of the mass is in collapsed clumps.

We illustrate this in Figure 5, where we plot (dotted line) the fraction of the final DWARF halo gas that resides in collapsed structures, as quantified by the condition $\rho > 10 \rho_{crit}(z)$. By this rather strict measure, half the DWARF gas is already in collapsed structures prior to $z \sim 2$, although by then the most massive halo progenitor (solid line) has only about $\sim 25\%$ of the final mass. This early aggregation of the halo gas into dense structures prevents it from being shock-heated by the pancake-driven shocks, reducing further the pre-virialisation heating efficiency.

4.3 Photoheating

As shown in Figure 4, the baryon fraction may be reduced because of heating by a photoionising background, but the effect (at $z = 0$) is restricted to haloes with virial temperatures $\lesssim 2.2T_{floor}$. This implies that ionising photons, which are unlikely to heat the gas to temperatures much higher than $\sim 2 \times 10^4$ K are only able to influence the formation of galaxies in haloes less massive than $\sim 10^{10}$ h^{-1} M$_\odot$. Our results for the baryon fraction in this case are well described by Eqn. 1, but with the revised parameters suggested by M05 for their photoheating model: $\alpha = 3$ and $M_c = 1.7 \times 10^9$ h^{-1} M$_\odot$; we show this fit in Figure 4 as a solid line.

The results shown in Figure 4 agree with those of Hoeft et al. (2006), who used a more detailed treatment of the UV background; the similarity of our findings is rather encouraging. We concur with their assessment that the characteristic mass scale of photoevaporation is probably considerably lower than derived from the filtering mass formalism of Gnedin (2000). Thus, although photoheating can reduce the baryon fraction in low-mass systems, it appears to be less efficient at shaping the extreme faint end of the galaxy luminosity function than previously inferred through semi-analytic modelling (e.g. Benson et al. 2002; Somerville 2002).

Our results seem to be robust to numerical resolution, as shown by the good agreement between the baryon fraction of the LOW-MASS and the DWARF haloes plotted in Figure 4. In the latter case, photoheating reduces the baryon fraction by 50% but there is no evidence that pre-virialisation has played a rôle; indeed, inspection of the evolution of the collapsed gas fraction (red dashed line in Figure 5) shows no discernible feature that may be associated with the collapse of the large-scale structure.

M05's pre-virialization model, shown as a dotted line in Figure 4, requires baryon fractions to be halved in haloes as massive as 5×10^{11} M$_\odot$; this is an order of magnitude larger than the mass of haloes significantly affected by photoheating and pre-virialisation in our simulations. Our results suggest, then, that other feedback mechanisms are required to match the faint end of the galaxy luminosity function in the ΛCDM scenario.

4.4 Application to cluster surveys

Our HIGH-MASS simulation also features over $115,000$ galaxy cluster-sized haloes, and demonstrates that, in the non-radiative regime, cluster baryon fractions are independent of virial mass, display little dispersion, and do not evolve significantly over the redshift range $0 < z < 1$. Observationally, mass profiles of clusters are typically only estimated reliably out to a maximum radius of r_{500}; the results within that radius are very similar to those plotted in Figure 2 at the virial radius. In haloes where the region interior to r_{500} is resolved by at least 500 dark matter particles, the mean cluster baryon fraction within r_{500} at $z = 0$ remains approximately 90% of the cosmic mean, again with an rms dispersion of $\sim 6\%$.

The key to the applicability of our results to cosmological tests is the validity of our non-radiative treatment of the ICM. Whilst the failure of purely non-radiative models to match some of the global scaling relations exhibited by clusters is well documented (e.g. Evrard & Henry 1991; Kaiser 1991; Navarro et al. 1995; Eke et al. 1998), this does not necessarily imply that non-radiative models give the wrong fraction of hot baryons in observed clusters. Since the ρ^2 dependence of thermal bremsstrahlung implies that the X-ray emissivity of clusters is dominated by the central region, it is possible to obtain agreement with the observed X-ray scaling relations by modifying only the central gas density (for instance, with radiative cooling or AGN feedback), whilst leaving the density of the bulk of the gas unchanged (e.g. Balogh et al. 1999; Voit et al. 2002, 2003; McCarthy et al. 2002, 2004).

It should be noted, however, that the X-ray luminosity-temperature relation can also be explained by models that do affect baryons at large radii (e.g. Kay et al. 2004; Kravtsov et al. 2005; Ettori et al. 2006). In such models the hot baryon fraction at r_{500} can be reduced by up to $\sim 30\%$, even for clusters with $M_{200} > 10^{15}$ h^{-1} M$_\odot$. However, such large-scale reductions by means of cooling and star formation conflict with optical constraints (e.g. Balogh et al. 2001), and the necessary level of feed-

back from SNe also appears unfeasibly high (Benson et al. 2003; Scannapieco & Oh 2004).

The effect of non-gravitational processes on the large-scale properties of rich clusters remains a source of debate. We anticipate that analyses of the large samples of rich clusters provided by the *Chandra* and *XMM-Newton* observatories will foster the development of a definitive picture of the ICM. This picture may well show that baryons at large radii are only minimally affected by non-gravitational processes, thus validating our results that rich cluster baryon fractions do not evolve for $z < 1$ and exhibit little dispersion.

5 CONCLUSIONS

We have measured the baryon fractions of a large sample of haloes drawn from a suite of non-radiative gas-dynamical simulations of the ΛCDM cosmology. The haloes span five orders of magnitude in virial mass, from dwarf galaxy haloes to large clusters. Within the virial radius, the baryon fraction averages 90% of the cosmic mean, with a fairly small dispersion ($\sim 6\%$ rms) and shows no dependence on redshift for well-resolved systems. This is at odds with the 'pre-virialisation' gravitational heating proposed by Mo et al. (2005). Pre-virialisation, if at all present, plays only a minor role in setting the budget of baryons that accrete into low-mass haloes.

Photoheating, modelled here as resulting from a uniform temperature 'floor' of 2×10^4 K imposed on the baryons from $z = 11$, is only able to reduce the baryon fraction in haloes with virial temperatures comparable to the photoheating floor. The absence of a strong mass trend in the baryon fractions of low mass haloes highlights the need for non-gravitational feedback as a means to regulate gas cooling and star formation in low-mass haloes, in order to reconcile the ΛCDM halo mass function with the observed galaxy luminosity function.

At r_{500}, the typical maximum radius at which current X-ray observatories can probe cluster temperatures, the baryon fraction remains similar to that at r_{200}, again with similarly small dispersion. Provided the effects of non-gravitational physics within r_{500} on rich cluster baryon fractions are small, we conclude that measurements of the matter density parameter and the dark energy equation of state based on cluster baryon fractions should not suffer from large uncertainties arising from the dispersion of baryon fractions, nor from redshift dependent systematics.

REFERENCES

Allen S. W., Schmidt R. W., Ebeling H., Fabian A. C., van Spey-broeck L., 2004, MNRAS, 353, 457

Balogh M. L., Babul A., Patton D. R., 1999, MNRAS, 307, 463

Balogh M. L., Pearce F. R., Bower R. G., Kay S. T., 2001, MN-RAS, 326, 1228

Benson A. J., Bower R. G., Frenk C. S., Lacey C. G., Baugh C. M., Cole S., 2003, ApJ, 599, 38

Benson A. J., Lacey C. G., Baugh C. M., Cole S., Frenk C. S., 2002, MNRAS, 333, 156

Blumenthal G. R., Faber S. M., Primack J. R., Rees M. J., 1984, Nature, 311, 517

Bower R. G., Benson A. J., Malbon R., Helly J. C., Frenk C. S., Baugh C. M., Cole S., Lacey C. G., 2006, MNRAS, 370, 645

Bullock J. S., Kravtsov A. V., Weinberg D. H., 2000, ApJ, 539, 517

Cole S., 1991, ApJ, 367, 45

Cole S., Lacey C. G., Baugh C. M., Frenk C. S., 2000, MNRAS, 319, 168

Croton D. J., Springel V., White S. D. M., De Lucia G., Frenk C. S., Gao L., Jenkins A., Kauffmann G., Navarro J. F., Yoshida N., 2006, MNRAS, 365, 11

Davis M., Efstathiou G., Frenk C. S., White S. D. M., 1985, ApJ, 292, 371

Efstathiou G., 1992, MNRAS, 256, 43P

Eke V. R., Navarro J. F., Frenk C. S., 1998, ApJ, 503, 569

Ettori S., Dolag K., Borgani S., Murante G., 2006, MNRAS, 365, 1021

Evrard A. E., Henry J. P., 1991, ApJ, 383, 95

Frenk C. S., Evrard A. E., White S. D. M., Summers F. J., 1996, ApJ, 472, 460

Frenk C. S., et al., 1999, ApJ, 525, 554

Gnedin N. Y., 2000, ApJ, 542, 535

Hoeft M., Yepes G., Gottlöber S., Springel V., 2006, MNRAS, 371, 401

Kaiser N., 1991, ApJ, 383, 104

Kang X., Jing Y. P., Mo H. J., Börner G., 2005, ApJ, 631, 21

Kauffmann G., Colberg J. M., Diaferio A., White S. D. M., 1999, MNRAS, 303, 188

Kay S. T., Thomas P. A., Jenkins A., Pearce F. R., 2004, MNRAS, 355, 1091

Kravtsov A. V., Nagai D., Vikhlinin A. A., 2005, ApJ, 625, 588

Lacey C., Cole S., 1993, MNRAS, 262, 627

Mac Low M.-M., Ferrara A., 1999, ApJ, 513, 142

McCarthy I. G., Babul A., Balogh M. L., 2002, ApJ, 573, 515

McCarthy I. G., Balogh M. L., Babul A., Poole G. B., Horner D. J., 2004, ApJ, 613, 811

Mo H. J., Yang X., van den Bosch F. C., Katz N., 2005, MNRAS, 363, 1155

Navarro J. F., Frenk C. S., White S. D. M., 1995, MNRAS, 275, 720

—, 1996, ApJ, 462, 563

—, 1997, ApJ, 490, 493

Navarro J. F., White S. D. M., 1993, MNRAS, 265, 271

Pen U.-L., 1997, New Astronomy, 2, 309

Power C., Navarro J. F., Jenkins A., Frenk C. S., White S. D. M., Springel V., Stadel J., Quinn T., 2003, MNRAS, 338, 14

Press W. H., Schechter P., 1974, ApJ, 187, 425

Quinn T., Katz N., Efstathiou G., 1996, MNRAS, 278, L49

Richstone D., Ajhar E. A., Bender R., Bower G., Dressler A., Faber S. M., Filippenko A. V., Gebhardt K., Green R., Ho L. C.,

Kormendy J., Lauer T. R., Magorrian J., Tremaine S., 1998, Nature, 395, A14+

Sasaki S., 1996, PASJ, 48, L119

Scannapieco E., Oh S. P., 2004, ApJ, 608, 62

Schaye J., Theuns T., Rauch M., Efstathiou G., Sargent W. L. W., 2000, MNRAS, 318, 817

Somerville R. S., 2002, ApJ, 572, L23

Somerville R. S., Primack J. R., 1999, MNRAS, 310, 1087

Spergel D. N., et al., 2006, ApJ, submitted, (astroph/0603449)

Springel V., 2005, MNRAS, 364, 1105

Springel V., et al., 2005, Nature, 435, 629

Strickland D. K., Stevens I. R., 2000, MNRAS, 314, 511

Vikhlinin A., Kravtsov A., Forman W., Jones C., Markevitch M., Murray S. S., Van Speybroeck L., 2006, ApJ, 640, 691

Voit G. M., Balogh M. L., Bower R. G., Lacey C. G., Bryan G. L., 2003, ApJ, 593, 272

Voit G. M., Bryan G. L., Balogh M. L., Bower R. G., 2002, ApJ, 576, 601

White S. D. M., Frenk C. S., 1991, ApJ, 379, 52

White S. D. M., Navarro J. F., Evrard A. E., Frenk C. S., 1993, Nature, 366, 429

White S. D. M., Rees M. J., 1978, MNRAS, 183, 341

This paper has been typeset from a T$_{\rm E}$X/ L$^{\rm A}$T$_{\rm E}$X file prepared by the author.